Supporting Information

Construction of Synergistic Pt Dual Active Sites Catalyst for Promoting Low Temperature CO Oxidation

Huixia Li,*[, a] Shaofan Fang[a], Shan Li[a], and Xuebo Chen*[,a,b]

[a] Shandong Laboratory of Advanced Materials and Green Manufacturing at Yantai, Yantai 264003 (P. R. China)

[b] College of Chemistry, Beijing Normal University, Beijing, 100091 (P. R. China)

Table of contents

Experimental Section

Chemicals and Materials

Cobalt nitrate hexahydrate ($Co(NO_3)_2·6H_2O$), Aluminum nitrate nonahydrate ($Al(NO_3)_3·9H_2O$), and Cerium nitrate hexahydrate ($Ce(NO_3)_3·6H_2O$) were purchased from Shanghai Macklin Biochemical Co. Ltd. The Chloroplatinic acid hexahydrate ($H_2PtCl_6·6H_2O$, Pt⩾37.5%) and urea were purchased from Shanghai Aladdin Biochemical Technology Co., Ltd. All chemicals and solvents were of reagent grade and used without further purification.

Synthesis of CoAlO nanosheets

CoAlO nanosheets as the support were prepared as follows. Briefly, 11.0 g of $Co(NO_3)_2·6H_2O$, 4.7 g of $Al(NO_3)_3·9H_2O$, and 30.00 g of urea (a molar ratio of Co^{2+}/Al^{3+}/urea of 3:1:40) were dissolved into 200 mL of deionized water. Then, the mixture was heated at 90 ℃ for 24 h by water bath. After cooling to room temperature, the product was collected by extraction filtration, washed with deionized water, and then dried at 60 °C for 12 h to obtain layered CoAl-LDH. Finally, the prepared CoAl-LDH was subjected to a calcination treatment at 500 °C in air for 4 h to get the CoAlO support.

Synthesis of different $xCeO_2$-CoAlO (20%, 40%, 60% and 80%) hybrid-oxides.

$xCeO_2$-CoAlO oxide supports were synthesized by the wet impregnation method. Initially, 0.5 g of CoAlO powder and varying contents of Ce precursor (40mg/mL $Ce(NO_3)_3·6H_2O$ solution) were dispersed in 50 ml of deionized water and stirred for 2 hours at 70 °C. The different amount of Ce was set to (20 wt.%, 40 wt.%, 60 wt.% and 80 wt %) with respect to the calculated amount of CoAlO powder. The solution was dried at 110 °C for 12 hours and calcined in air at 500 °C for 8 hours with a heating rate of 2 $°C·min^{-1}$.

Synthesis of the CeO_2 support.

Cerium nitrate was placed in a crucible and calcined in a muffle oven at 500 ℃ for 8h.

Synthesis of the Pt/xCeO_2-CoAlO (20%, 40%, 60% and 80%)， Pt/CoAlO and Pt/CeO_2 catalysts.

To synthesize Pt supported catalysts, varying amounts of H_2PtCl_6 solution was added to 50 mL of deionized water with 0.5 g of xCeO_2-CoAlO (20%, 40%, 60% and 80%), CoAlO and CeO_2 powder. The mixed solution is stirring for 2h and standing for 12h. Then, the precipitate was filtrated and washed with distilled water several times. Subsequently, the solid was dried in a oven at 110 ℃ overnight and calcined at 500 ℃ for 3 h in 10%H_2/Ar atmosphere. The initial amount of Pt was set to 0.5 wt.% with respect to the total weight of xCeO_2-CoAlO. The synthesized catalysts were named as Pt/20CeO_2-CoAlO, Pt/40CeO_2-CoAlO, Pt/60CeO_2-CoAlO, Pt/80CeO_2-CoAlO, Pt/CoAlO and Pt/CeO_2. The prepared process of the other loading amount of Pt, such as 0.1 wt and 1 wt%, is similar to that of 0.5 wt% Pt.

Catalyst characterizations.

A transmission electron microscopy (TEM, Tecnai G2 S-Twin F20) with model of Tecnai G2 S-Twin F20) was adopted to research the micromorphology and structure. Elemental mapping analysis was implemented using a scanning TEM (STEM) and on a FEI Talos system equipped with a 200 kV FEG. The powder X-ray diffraction (XRD) patterns of the catalysts were collected by Rigaku Miniflex apparatus equipped with a Cu-Kα radiation (λ=1.5418 Å) at 40 kV and 40 mA. X-ray photon-electronic spectroscopy (XPS; Thermo Scientific ESCALAB 250, X-ray source) measurements were used for determine the valence states of various elements. C1s photoemission line at a binding energy of 284.8 eV was used to calibrate the charging shift. To obtain the specific

surface areas of the catalysts, nitrogen adsorption-desorption isotherms were measured by an asap2020 analyzer. O_2 temperature–programmed desorption (O_2-TPD) experiments and H_2 temperature programmed reduction techniques (H_2-TPR) profiles experiments of the samples (~30 mg) were performed on a quartz reactor and recorded by a Micromeritics AutoChem II 2920 Apparatus with Thermal Conductivity Detector (TCD). For H_2-TPR test, the sample was weighed and placed in a U-shaped quartz tube. The sample was heated at 10 ℃/min from room temperature to 200 ℃ for drying pre-treatment. The sample was purged by He air flow (50 mL /min) for 1h, cooled to 50 ℃, and injected with 10% H_2/Ar mixture (50 mL/min) for 0.5h after baseline stabilization. The sample was desorbed at 800 ℃ at 10 ℃/min in 10% H_2/Ar flow, and the reduction gas was detected by TCD. For O_2-TPD test, The sample was heated at 10℃/min from room temperature to 200 ℃ for drying pre-treatment, He air flow (50 mL /min) was purged for 1h, cooled to 50 ℃, and 10% O_2/He mixture (30-50 mL /min) was injected for 1h to saturation. Switching He air flow (50 mL /min) to purge the surface for 1 h to remove the weak physical adsorption O_2, and finally in He atmosphere at a temperature rise of 10 ℃ /min to 800 ℃ desorption, using TCD to detect the exfiltration gas. Chemical compositions of samples were analyzed by inductively coupled plasma-optical emission spectroscopy (ICP-OES, PerkinElmer). Nitrogen adsorption isotherms of the samples were measured using an asap2020 analyzer. Specific surface areas of samples were calculated using linear portion of adsorption branch of the isotherms. Pore size and pore volume analysis of samples were carried out with BJH method using desorption branch of the isotherms. The X-band electron paramagnetic resonance (ESR) spectra results were obtained at room time on a BRUKER EMX Plus X-band spectrometer. The extended X-ray absorption fine structure (EXAFS) measurements were carried out on the sample at

beamline 07A1 of Taiwan Light Source (TLS) of National Synchrotron Radiation Research Center (NSRRC). This beamline adopted fixed-exit double crystal Si (111) monochromator to ranging the X-ray energy from 5-23 keV. The end-station equipped three ionization chambers and Lytle detector for transmission and fluorescence mode X- ray absorption spectroscopy.The beam size of X- ray on the sample is about 0.5×0.25 mm (HxV) with flux higher than 1×10^{10} photon/sec. The results were processed by employing the Athena software.

In situ X-ray photoelectron spectra (in situ XPS) were recorded using an ESCALAB 250Xi spectrometer with a monochromatic Al anode Kα radiation (1486.6 eV), and the charging effects were corrected by setting the C1s binding energy of the adventitious carbon to 284.8 eV. The catalyst was first subjected to vacuum treatment at 180 ^{o}C, and then XPS spectra were collected. Afterward, CO gas (1% CO) was introduced into the reactor until stabilization. The XPS spectra were collected again. Following this, a mixture of CO and O_2 gas (1% CO + 20% O_2) was introduced into the reactor, and the XPS spectra of were collected once more. When the XPS spectra were collected, the sample was directly moved to analysis chamber without being exposed to the environment.

In situ diffuse reflectance Fourier transform infrared spectroscopy (DRIFTS) was carried out using 1% CO, 20% O_2 and He balance as reaction gas. The spectra of samples were recorded using a Nicolet iS50 FT-IR spectrometer equipped with Harrick DRIFTS accessory and Harrick high temperature reaction chamber. Prior to the measurement, the catalysts (about 10 mg) were treated in-situ at 200 ^{o}C in pure N_2 with a flow rate of 40 mL·min^{-1} to remove the contaminants on surface of catalyst. A background spectrum was collected for correction after cooling to 30 ^{o}C. Then, the reaction gas was introduced into the in-situ chamber at a flow rate of 10 mL·min^{-1}. The

spectra were averaged over 48 scans with a resolution of 4 cm^{-1}.

Electrochemical Measurement: Carbon monoxide (CO) stripping was carried out following the method reported by Gan et al.[1] Electrochemical measurements were performed in a three-compartment glass cell with a rotating disk electrode and Chenhua 760e electrochemical workstation, using Ag/AgCl as the reference electrode and a Pt gauze as the counter electrode.

Catalytic Activity Test of CO Oxidation.

Catalytic activity of the as-prepared catalysts was measured in a feed reactor. The feed contained 1 % CO, 20 % O_2, and the balance He at a rate of 1×10^3 $cm^3 \cdot min^{-1} \cdot g^{-1}$ (roughly 60000 h^{-1} GHSV). To compare the long-time stability for supported Pt catalysts at a high temperature, the test was performed under a mix-gas of CO oxidation at 180 °C for 50h. The products and reactants were analyzed by a gas chromatograph equipped with TC-detector. No products other than those resulted gas from CO, i.e., CO_2 were observed under the applied reaction conditions. Basically, the percentage of conversion in CO oxidation process are defined as

$$X_{CO}(\%) = \frac{F_{CO}^{in} - F_{CO}^{out}}{F_{CO}^{in}} \times 100$$

where X represent percentage conversion, F is the molar flow of the indicated gas (inlet or outlet), respectively.

The reaction rate k ($\mu mol \cdot s^{-1} \cdot g^{-1}$) can be calculated by assuming ideal gas behavior:

$$k = \frac{Xco * Fco}{W} \times 100\%$$

where, X_{CO} is CO conversion, F_{CO} ($\mu mol \cdot s^{-1}$) is molar gas flow rate of CO, and W (g) is the mass of catalyst in the fixed-bed reactor.

The catalytic velocities were determined by a turnover frequency of CO conversion over Pt sites

(TOF_{Pt} (s^{-1})), which can be obtained by the following equation:

$$TOF_{Pt} = \frac{Xco * Fco}{N_{Pt}} \times 100\%$$

where, X_{CO} is CO conversion (<20%), F_{CO} (μmol·s^{-1}) is molar gas flow rate of CO, and N_{Pt} (μmol) is the total number of Pt atoms on the catalyst. It should be noted that all the catalysts used in this study contained 0.5 wt% Pt. Moreover, all Pt atoms were considered when calculating TOF_{Pt} to enable a fair comparison of catalyst activity under the same Pt usage.

The apparent activation energies (Ea (kJ · mol^{-1})) over the catalysts were calculated at CO conversion lower than 20% according to the Arrhenius equation.

DFT Calculation.

Spin-polarized DFT calculations were performed using the Vienna ab initio simulation package (VASP)[2,3]. The generalized gradient approximation proposed by Perdew, Burke, and Ernzerhof (GGA-PBE) is selected for the exchange-correlation potential[4]. The pseudo-potential was described by the projector-augmented-wave (PAW) method[5]. The geometry optimization is performed until the Hellmann–Feynman force on each atom is smaller than 0.02 eV·$Å^{-1}$. The energy criterion is set to 10^{-6} eV in iterative solution of the Kohn-Sham equation. To model Pt/CeO_2-CoAlO, single Pt atom and Pt cluster consisting of 4 atoms were chosen on the CeO_2-CoAlO heterostructure, respectively. The repeated slabs were separated from their neighboring images by a 13 width vacuum in the direction perpendicular to the surface. The Pt or Pt cluster-only cell size is a*b*c=5.7*19.4*17.4 $Å^3$, while the one containing both Pt and Pt cluster is 11.4*15.0*17.4 $Å^3$.

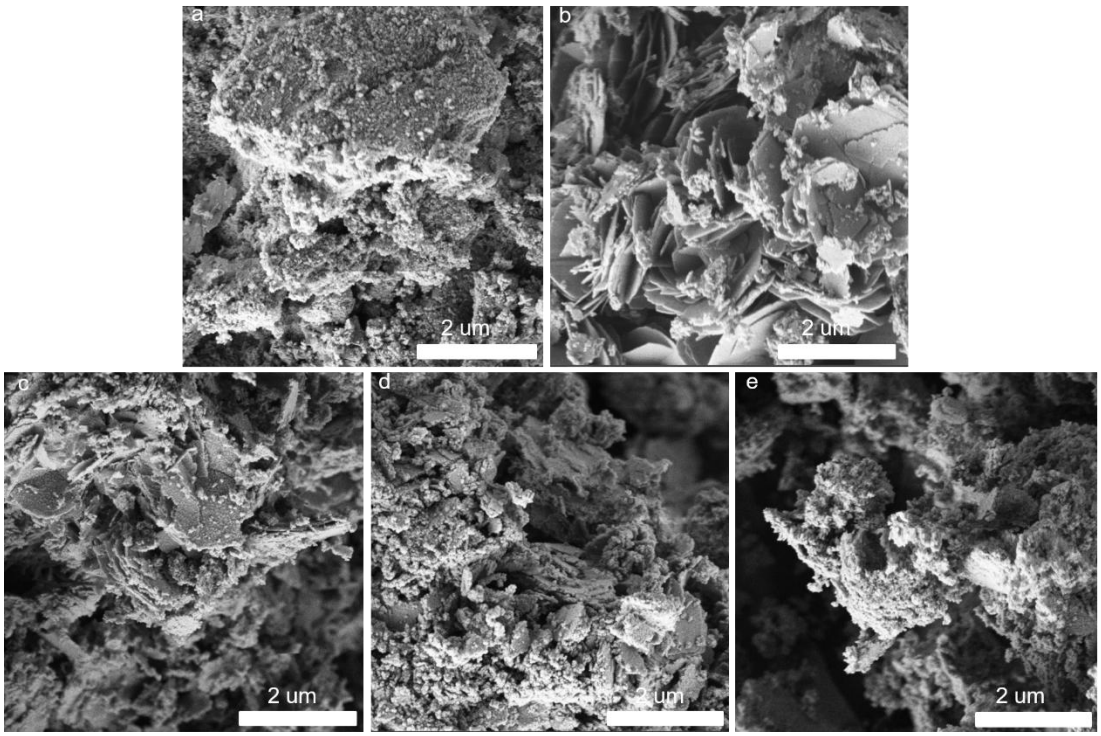

Figure S1. SEM images of the samples Pt/CeO_2, Pt/CoAlO, Pt/20CeO_2-CoAlO, Pt/40CeO_2-CoAlO and Pt/80CeO_2-CoAlO.

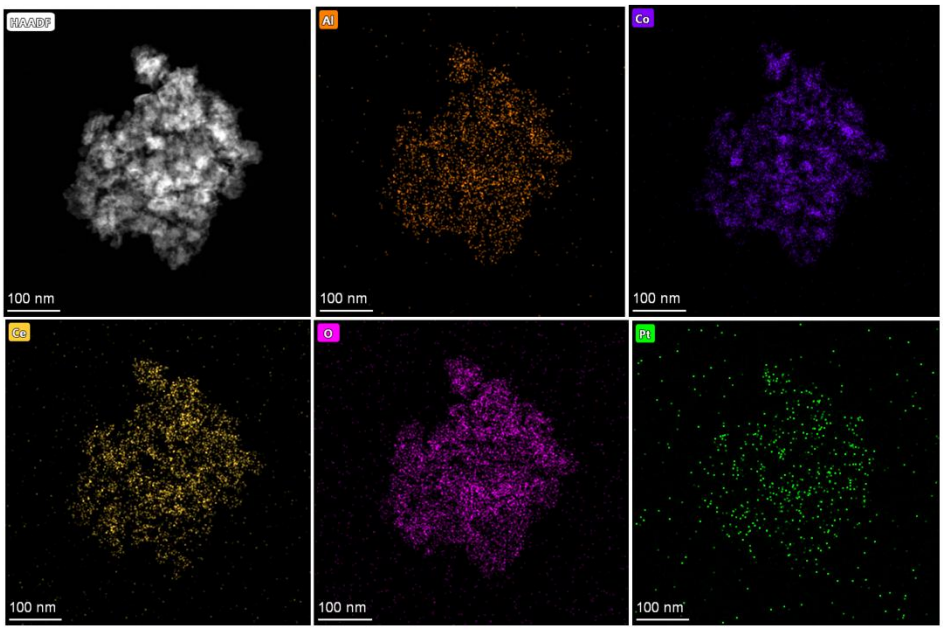

Figure S2. HAADF-STEM of Pt/60CeO_2-CoAlO with element distribution images corresponding to Al, Co, Ce, O and Pt.

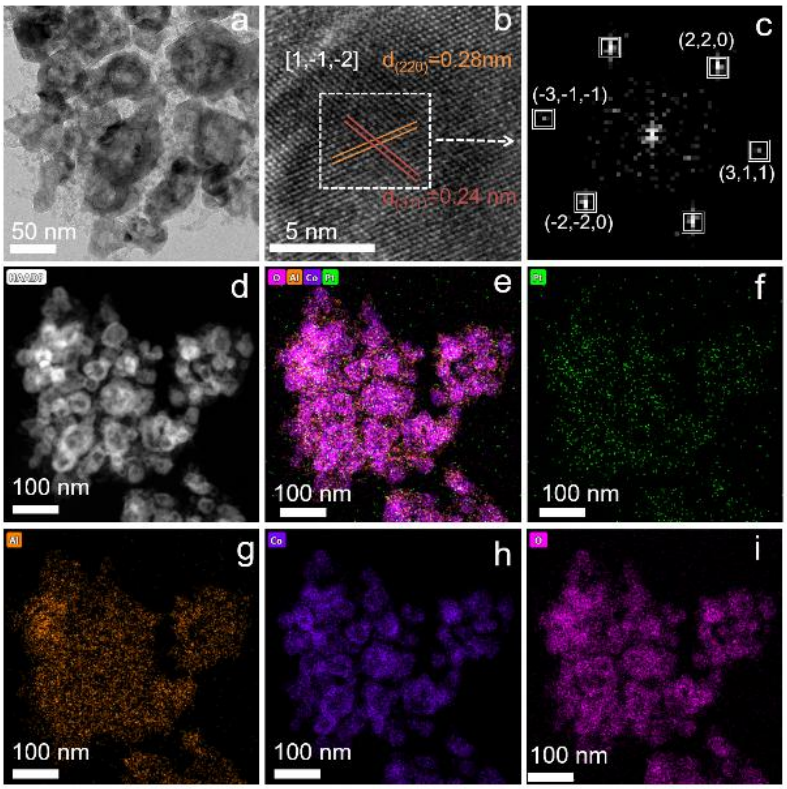

Figure S3. Preparation and morphological characterization: (a) TEM, (b) HR-TEM images, (c) the fast Fourier transform (FFT) pattern of the rectangle region, (d) HADDF-STEM image and the corresponding elemental mapping of (e) Pt+Co+Al+O, (f) Pt, (g) Al, (h) Co, (i) O for the Pt/CoAlO catalyst.

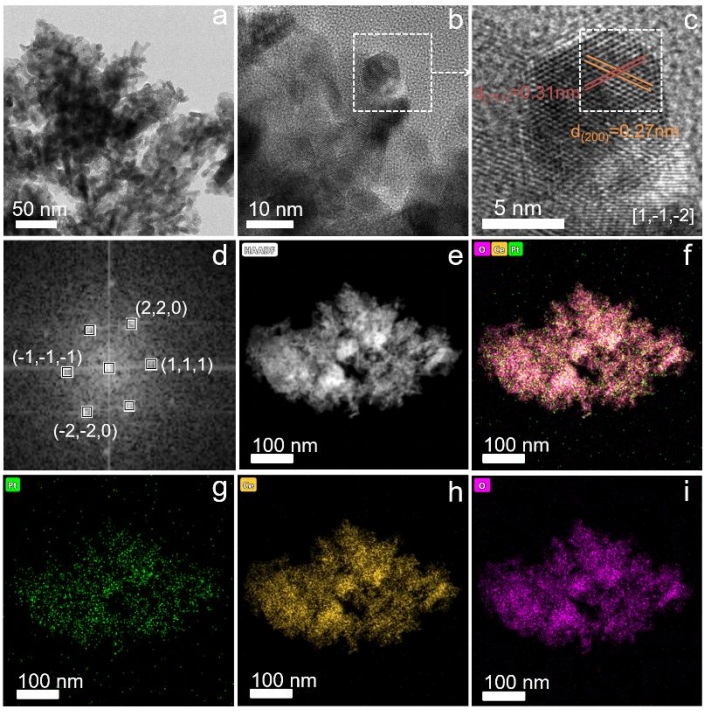

Figure S4. (a) TEM, (b, c) HR-TEM images, (d) the fast Fourier transform (FFT) pattern of the rectangle region, (e) HADDF STEM image and the corresponding elemental mapping of (f) Pt+Ce+O, (g) Pt, (h) Ce and (i) O for the Pt/CeO_2 catalyst.

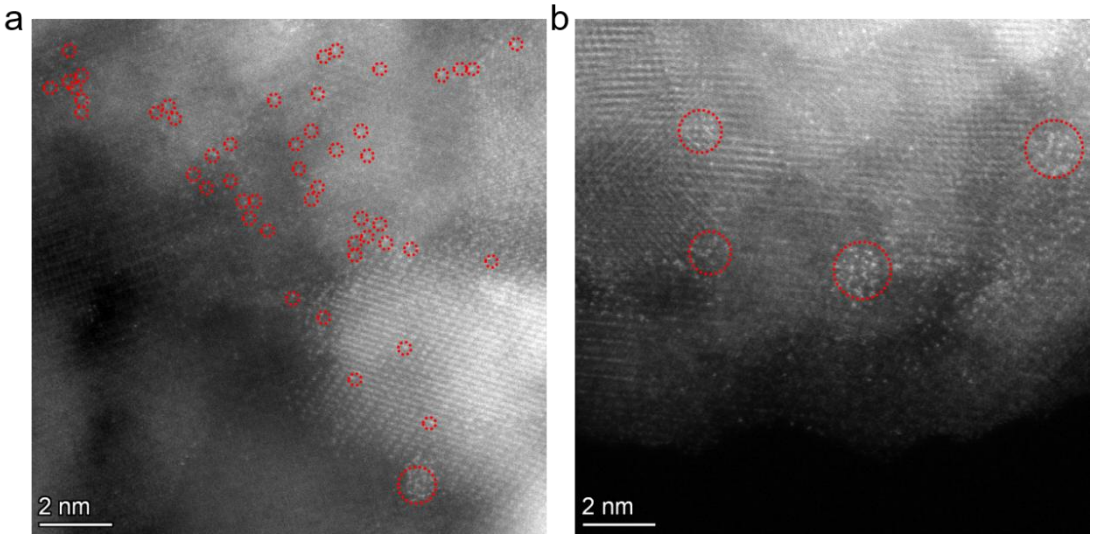

Figure S5. (a, b) the AC HAADF-STEM images of Pt/60CeO_2-CoAlO catalyst.

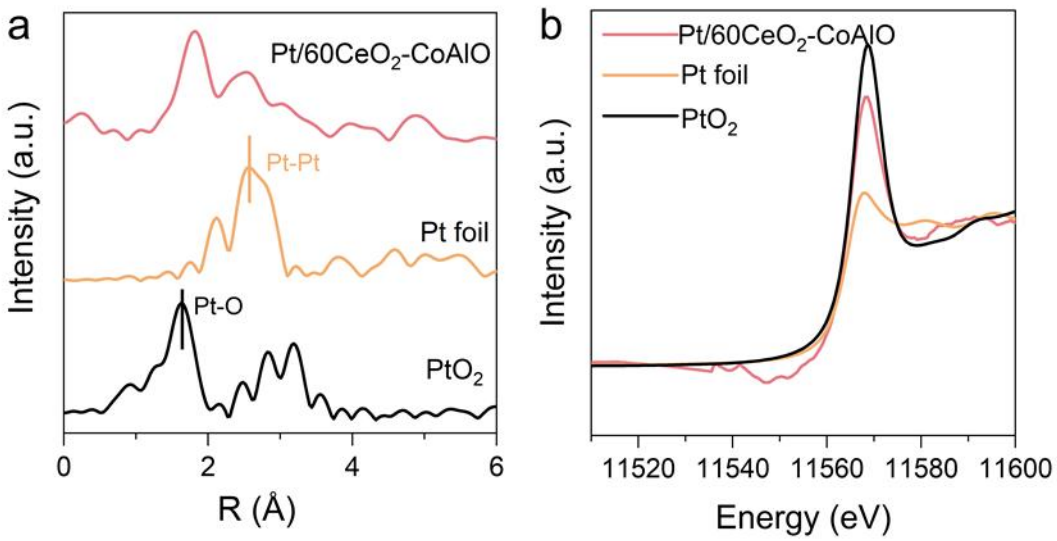

Figure S6. (a) k^2-weighted Fourier transform spectra from EXAFS and (b) Normalized Pt L_3-edge XANES spectra of Pt foil, PtO_2 and Pt/60CeO_2-CoAlO.

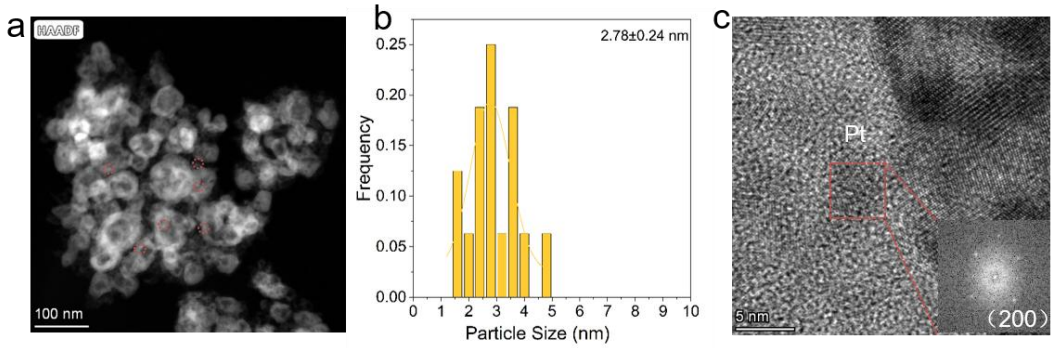

Figure S7. HAADF-STEM images, the diagram of size distribution and HR-TEM images of Pt/CoAlO.

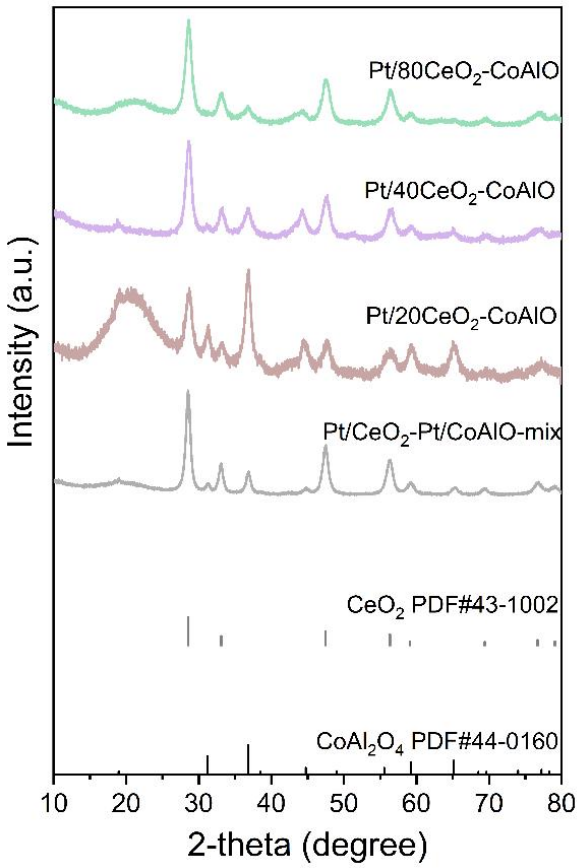

Figure S8. The XRD patterns of Pt/CeO_2-Pt/CoAlO-mix, Pt/20CeO_2-CoAlO, Pt/40CeO_2-CoAlO and Pt/80CeO_2-CoAlO catalysts.

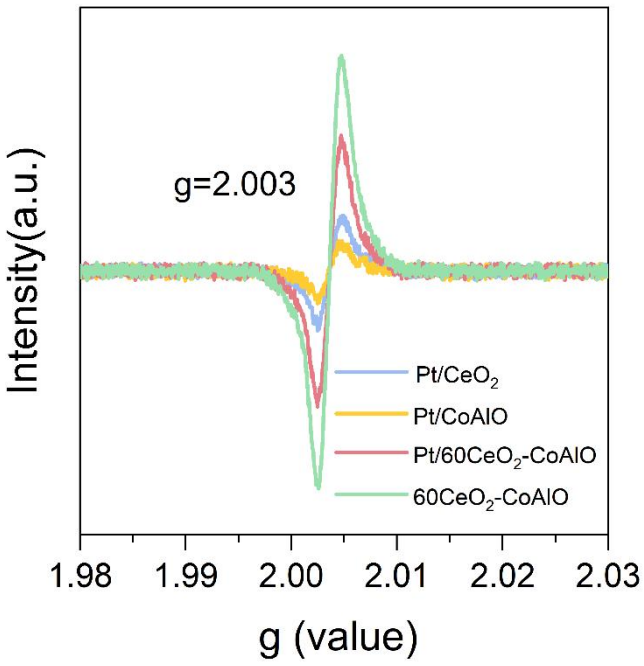

Figure S9. ESR profiles of $60CeO_2$-CoAlO support, Pt/$60CeO_2$-CoAlO, Pt/CoAlO and Pt/CeO_2 catalysts.

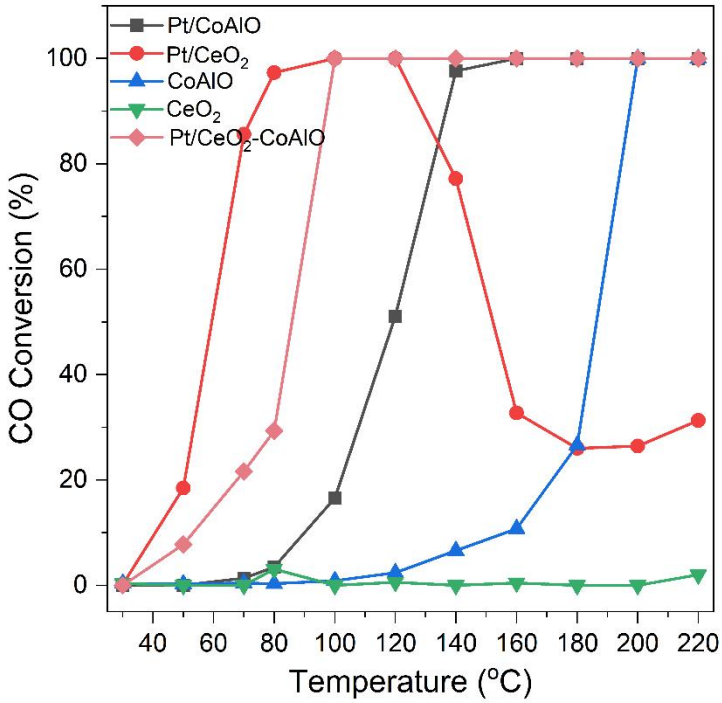

Figure S10. CO conversion of Pt/60CeO_2-CoAlO, Pt/CoAlO, Pt/CeO_2, CoAlO and CeO_2 catalysts.

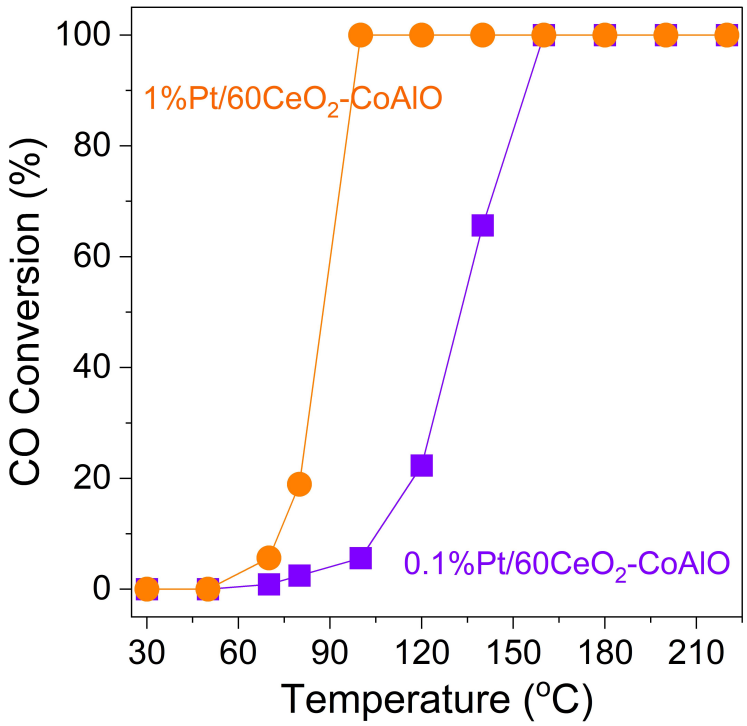

Figure S11. CO conversion of 0.1%Pt/60CeO_2-CoAlO and 1%Pt/60CeO_2-CoAlO catalysts.

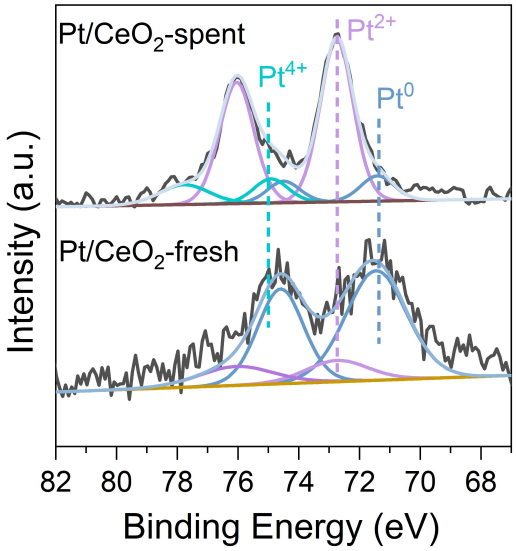

Figure S12. The XPS spectra of Pt4f for the fresh and used Pt/CeO_2 catalyst under the 1%CO+20%O_2, and He balance.

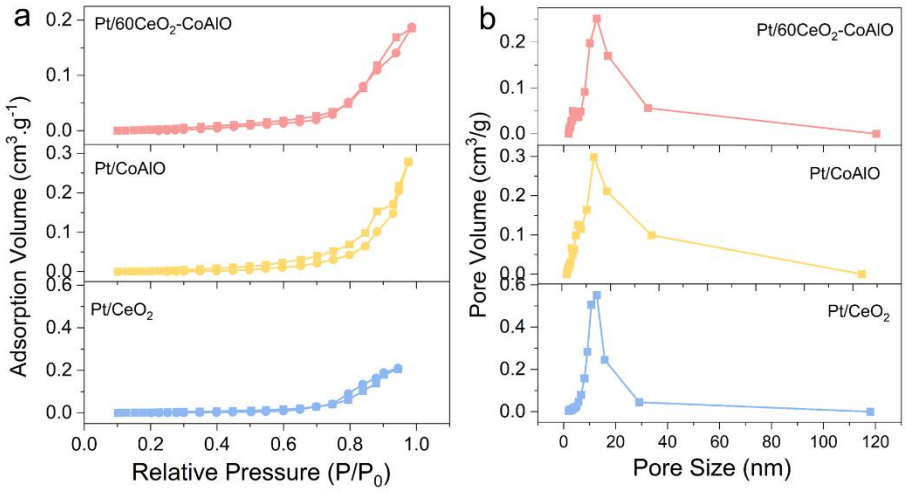

Figure S13. (a) N_2 adsorption−desorption curves and (b) the pore size distributions of Pt/60CeO_2-CoAlO, Pt/CoAlO and Pt/CeO_2.

To assess the porosity of all the catalysts, N_2 adsorption−desorption measurements were conducted. All samples gave a typical Type-IV isotherm with H3-type hysteresis loops over the relative pressure range, P/P_0 = 0.9-1 (Figure S13a), indicating a mesoporous feature according to the IUPAC classification[6]. No nitrogen adsorptions observed in lower relative pressure (P/P_0 = 0-0.9) demonstrate the absence of micropores for our samples. BJH pore size distribution curves for the samples also confirmed their mesopore feature, showing a pore size distribution from 2 to 5 nm (Fig. S13b). BET surface areas for samples Pt/60CeO_2-CoAlO, Pt/CoAlO and Pt/CeO_2 were 65, 79 and 85 m^2/g, respectively (Table S2). The surface area is little difference with the calcination temperature increasing. The overall textural properties are listed in Table S2.

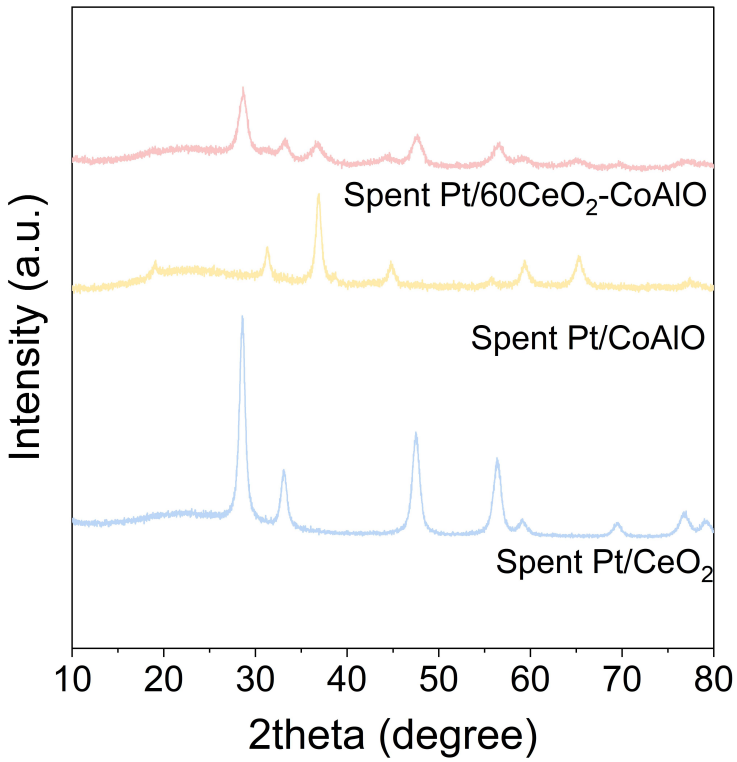

Figure S14. The XRD patterns of Pt/60CeO_2-CoAlO, Pt/CoAlO and Pt/CeO_2 catalysts after the CO oxidation reaction.

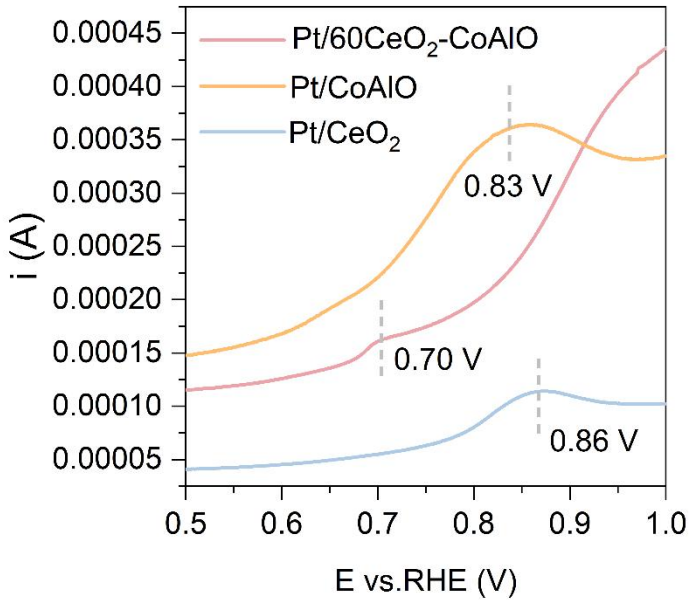

Figure S15. CO stripping voltammograms of Pt/60CeO_2-CoAlO, Pt/CoAlO and Pt/CeO_2 catalysts.

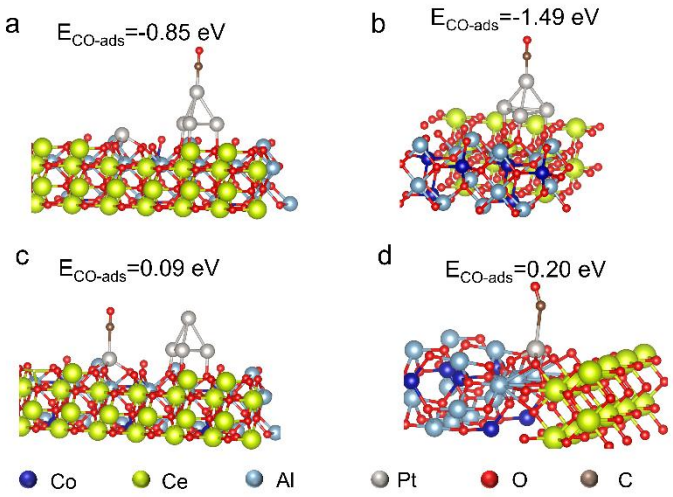

Figure S16. DFT calculation of the CO adsorption energy for (a) Pt clusters of the coexisted Pt single atoms and Pt clusters, (b) isolated Pt clusters, (c) Pt single atoms of the coexisted Pt single atoms and Pt clusters, and (d) isolated Pt atoms supported on the CeO_2-CoAlO, respectively.

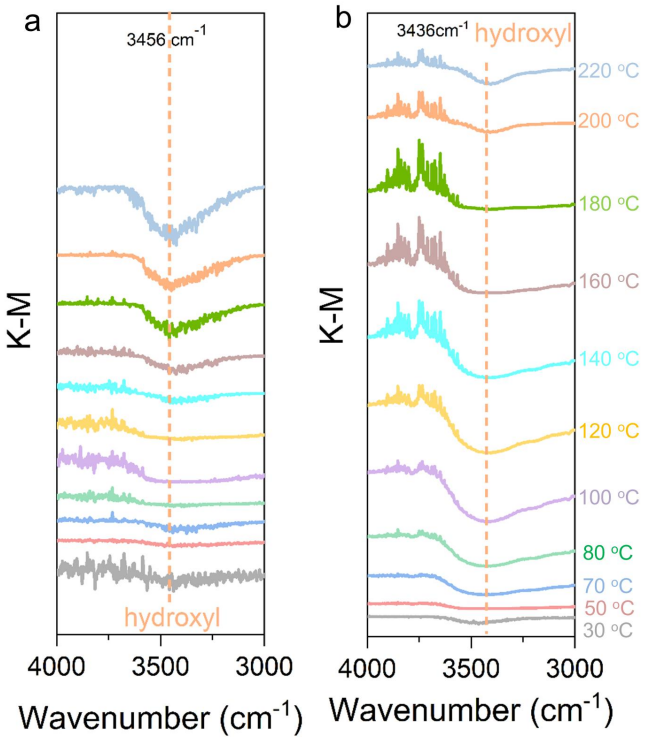

Figure S17. In situ DRIFT spectra in the range of 4000-3000 cm^{-1} for (a) Pt/CoAlO and (b) Pt/60CeO_2-CoAlO at different temperature under a continuous flow of the CO oxidation reaction gas (1% CO and 20% O_2 in He balance).

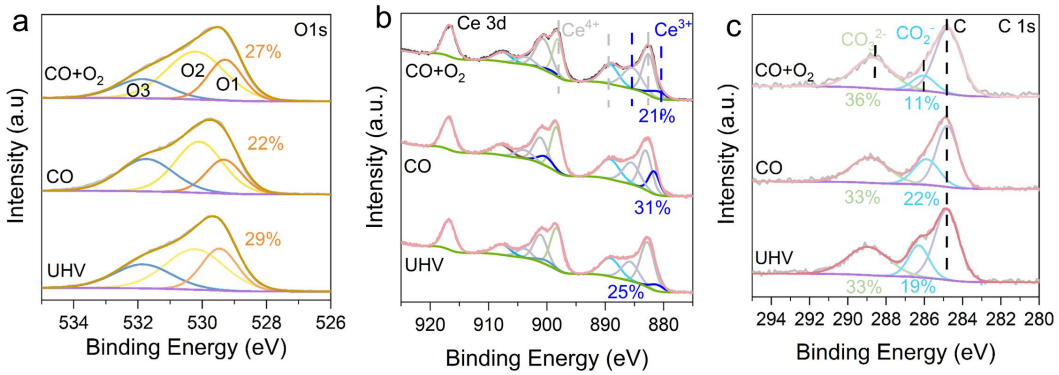

Figure S18. In situ XPS spectra of (a) O 1s, (b) Ce 3d and (c) C 1s of Pt/60CeO_2-CoAlO at 180 °C: in UHV, under 1%CO, under 1%CO and 20%O_2 conditions.

Table S1. Elemental compositions of the catalysts.

Sample	Nominal molar ratio (Co : Al)	Molar ratio[a] (Co : Al)	Pt nominal weight (%)	Pt weight[a] (%)	Ce weigh[a] (%)
Pt/CoAlO	3	3.77	0.5	0.47	0
Pt/20CeO_2-CoAlO	3	3.70	0.5	0.44	5.84
Pt/40CeO_2-CoAlO	3	3.66	0.5	0.46	10.2
Pt/60CeO_2-CoAlO	3	3.64	0.5	0.47	14.6
Pt/80CeO_2-CoAlO	3	3.63	0.5	0.46	16.4
Pt/CeO_2	-	-	0.5	0.45	-

[a]These values were determined by ICP.

Table S2. Particulate properties of the catalysts.

Sample	Surface area ($m^2 \cdot g^{-1}$)	Pore volume ($cm^3 \cdot g^{-1}$)	Pore diameter (nm)	Grain size of CeO_2[a]	Pt dispersion (%)[b]
Pt/CeO_2	79	0.21	10.63	11.28	83
Pt/CoAlO	85	0.28	13.01	-	35
$Pt/20CeO_2$-CoAlO	71	0.20	10.95	9.85	-
$Pt/40CeO_2$-CoAlO	66	0.19	11.50	9.46	-
$Pt/60CeO_2$-CoAlO	65	0.19	11.56	9.30	93
$Pt/80CeO_2$-CoAlO	79	0.22	11.09	8.96	-

[a]Calculated grain sizes from the Scherrer equation using the (111) diffraction peaks of CeO_2.

[b]Pt dispersion determined by CO pulse adsorption.

Table S3. Comparison of CO oxidation performance over Pt/60CeO_2-CoAlO and those Pt-based catalysts reported in literature.

Catalysts	Pt loading (wt%)	Composition of feed gas (%)			Maximal CO conversion (%) (T_{100})	TOF (s^{-1})	E_a (kJ/mol)	Ref.
		CO	O_2	He				
Pt/60CeO2-CoAlO	0.5	1	20	79	100	0.89	40.44	This work
Pt/80CeO_2-CoAlO	0.5	1	20	79	140	0.14	44.50	This work
Pt/40CeO_2-CoAlO	0.5	1	20	79	140	0.37	56.63	This work
Pt/20CeO_2-CoAlO	0.5	1	20	79	160	0.084	61.54	This work
Pt/CoAlO	0.5	1	20	79	160	0.0028	127.72	This work
Pt/CeO_2	0.5	1	20	79	80	-	-	This work
Pt/TiO_2	1	0.5	5	-	115	0.01	-	7
1Pt2Bi-SiO_2	1	1	20	-	-	-	50	8
Pt/CNT-600	1	1	20	-	100	0.05	26	9
Pt/CeO_2-Al_2O_3	1	1	1	-	76	0.22	-	10
Pt_1/CeO_x-TiO_2	0.25	1	4	-	200	0.093	-	11
Pt_1/m-Al_2O_3	0.2	2.5	2.5	-	200	0.023	-	12
Pt_1SAC/CeO_2	3	1sccm	1.5sccm	75sccm	180	0.072	-	13
Pt/Al_2O_3+Polydedra Ceria	1	1.5ml/min	1ml/min	75ml/min	225	0.15	56	14
Pt_1/ θ -Al_2O_3	0.18	1	1	-	200	0.013	-	15
Pt_1/FeO_x	0.17	1	1	-	27	0.136	-	16
Pt/TiO_2(B)	1	0.9	24	-	100	0.109	50.2	17
Pt/CeO_2-S	1	0.4	10	-	-	-	42.5	18

Reference

1. Wang, Z.; Yao, X.; Kang, Y.; Miao, L.; Xia, D.; Gan, L., Structurally Ordered Low - Pt Intermetallic Electrocatalysts toward Durably High Oxygen Reduction Reaction Activity. *Advanced Functional Materials* **2019**, 29 (35), 1902987.

2. G. Kresse, Comput. Efficiency of ab-initio total energy calculations for metals and semiconductors using a plane-wave basis set, *Mater. Sci.* **1996**, *6*, 15.

3. .G. Kresse, Efficient iterative schemes for ab initio total-energy calculations using a plane-wave basis set, *Phys. Rev. B*, **1996**, *54*, 11169.

4. J. P. Perdew, K. Burke and M. Ernzerhof, Generalized Gradient Approximation Made Simple, *Phy. Rev. Lett.*, **1996**, *77*, 3865.

5. P. Blöchl, Projector augmented-wave method, *Phys. Rev. B*, **1994**, *50*, 17953.

6. Wu, B.; Shan, C.; Zhang, X.; Zhao, H.; Ma, S.; Shi, Y.; Yang, J.; Bai, H.; Liu, Q., CeO_2/Co_3O_4 porous nanosheet prepared using rose petal as biotemplate for photo-catalytic degradation of organic contaminants. *Applied Surface Science*, **2021,** *543*.

7. Hojo, H.; Gondo, M.; Yoshizaki, S.; Einaga, H., Atomic and Electronic Structure of Pt/TiO_2 Catalysts and Their Relationship to Catalytic Activity. *Nano Letters*, **2021,** *22* (1), 145-150.

8. Nan, B.; Fu, Q.; Yu, J.; Shu, M.; Zhou, L.-L.; Li, J.; Wang, W.-W.; Jia, C.-J.; Ma, C.; Chen, J.-X.; Li, L.; Si, R., Unique structure of active platinum-bismuth site for oxidation of carbon monoxide. *Nature Communications*, **2021,** *12* (1), 3342.

9. Chen, W.; Cao, J.; Yang, J.; Cao, Y.; Zhang, H.; Jiang, Z.; Zhang, J.; Qian, G.; Zhou, X.; Chen, D.; Yuan, W.; Duan, X., Molecular-level insights into the electronic effects in platinum-catalyzed carbon monoxide oxidation. *Nature Communications,* **2021,** *12* (1), 6888.

10. Jeong, H.; Shin, D.; Kim, B. S.; Bae, J.; Shin, S.; Choe, C.; Han, J. W.; Lee, H., Controlling the Oxidation State of Pt Single Atoms for Maximizing Catalytic Activity. *Angewandte Chemie International Edition* **2020,** *59* (46), 20691-20696.

11. Yoo, M.; Yu, Y.-S.; Ha, H.; Lee, S.; Choi, J.-S.; Oh, S.; Kang, E.; Choi, H.; An, H.; Lee, K.-S.; Park, J. Y.; Celestre, R.; Marcus, M. A.; Nowrouzi, K.; Taube, D.; Shapiro, D. A.; Jung, W.; Kim, C.; Kim, H. Y., A tailored oxide interface creates dense Pt single-atom catalysts with high catalytic activity. *Energy & Environmental Science* **2020,** *13* (4), 1231-1239.

12. Zhang, Z.; Zhu, Y.; Asakura, H.; Zhang, B.; Zhang, J.; Zhou, M.; Han, Y.; Tanaka, T.; Wang, A.; Zhang, T.; Yan, N., Thermally stable single atom Pt/m-Al2O3 for selective hydrogenation and CO oxidation. *Nature Communications* **2017,** *8* (1).

13. Kunwar, D.; Zhou, S.; DeLaRiva, A.; Peterson, E. J.; Xiong, H.; Pereira-Hernández, X. I.; Purdy, S. C.; ter Veen, R.; Brongersma, H. H.; Miller, J. T.; Hashiguchi, H.; Kovarik, L.; Lin, S.; Guo, H.; Wang, Y.; Datye, A. K., Stabilizing High Metal Loadings of Thermally Stable Platinum Single Atoms on an Industrial Catalyst Support. *ACS Catalysis* **2019,** *9* (5), 3978-3990.

14. Jones, J.; Xiong, H.; DeLaRiva, A. T.; Peterson, E. J.; Pham, H.; Challa, S. R.; Qi, G.; Oh, S.; Wiebenga, M. H.; Pereira Hernández, X. I. J. S., Thermally stable single-atom platinum-on-ceria catalysts via atom trapping. **2016,** *353* (6295), 150-154.

15. Moses-DeBusk, M.; Yoon, M.; Allard, L. F.; Mullins, D. R.; Wu, Z.; Yang, X.; Veith, G.; Stocks, G. M.; Narula, C. K. J. J. o. t. A. C. S., CO oxidation on supported single Pt atoms: experimental and ab initio density functional studies of CO interaction with Pt atom on θ-Al_2O_3 (010) surface. **2013,** *135* (34), 12634-12645.

16. Qiao, B.; Wang, A.; Yang, X.; Allard, L. F.; Jiang, Z.; Cui, Y.; Liu, J.; Li, J.; Zhang, T. J. N. c.,

Single-atom catalysis of CO oxidation using Pt_1/FeO_x. **2011,** *3* (8), 634-641.

17. Liu, J.; Ding, T.; Zhang, H.; Li, G.; Cai, J.; Zhao, D.; Tian, Y.; Xian, H.; Bai, X.; Li, X., Engineering surface defects and metal–support interactions on Pt/TiO_2(B) nanobelts to boost the catalytic oxidation of CO. *Catalysis Science & Technology*, **2018,** *8* (19), 4934-4944.

18. Nie, L.; Mei, D.; Xiong, H.; Peng, B.; Ren, Z.; Hernandez, X. I. P.; DeLaRiva, A.; Wang, M.; Engelhard, M. H.; Kovarik, L. J. S., Activation of surface lattice oxygen in single-atom Pt/CeO_2 for low-temperature CO oxidation. **2017**, *358* (6369), 1419-1423.